This is a peer-reviewed, author's accepted manuscript of the following research article: Liu, X., Yu, Y., Li, F., & Durrani, T. S. (2022). Throughput maximization for RIS-UAV relaying communications.
IEEE Transactions on Intelligent Transportation Systems, 23(10), 19569-19574. https://doi.org/10.1109/tits.2022.3161698

Throughput Maximization for RIS-UAV Relaying Communications

Xin Liu, *Senior Member, IEEE,* Yingfeng Yu, Feng Li, *Member, IEEE,* and Tariq S Durrani, *Life Fellow, IEEE*

***Abstract*—In this paper, we consider a reconfigurable intelligent surface (RIS) assisted unmanned aerial vehicle (UAV) relaying communication system, where the RIS is mounted on the UAV and can move at a high speed. Compared with the conventional static RIS, better performance and more flexibility can be achieved with the assistance of the mobile UAV. We maximize the average downlink throughput by jointly optimizing the UAV trajectory, RIS passive beamforming and source power allocation for each time slot. The formulated non-convex optimization problem is decomposed into three subproblems: passive beamforming optimization, trajectory optimization and power allocation optimization. An alternating iterative optimization algorithm of the three subproblems is proposed to achieve the suboptimal solutions. The numerical results indicate that the RIS-UAV relaying communication system with trajectory optimization can get higher throughput.**

***Index Terms*—UAV, RIS, relaying communications, passive beamforming, throughput.**

I. Introduction

Due to the superiorities of high mobility, low cost and flexibility, unmanned ariel vehicle (UAV) has undergone rapid developments in both military and civilian fields, such as ariel photography, disaster rescue, inspection, etc. Recently, the UAV is playing an important role in the fifth-generation (5G) mobile communications owning to its wide coverage and line-of-sight (LoS) transmission [1]–[4]. In 5G, the UAV can be deployed as a relay, which will assist the ground communications in severe fading channel to improve the transmission performance [5]. However, the traditional UAV relay needs to forward the signals from the ground terminals with large transmit power resulting in the great consumption of the finite UAV energy.

Fortunately, reconfigurable intelligent surface (RIS) is recently proposed to improve communication performance while saving transmit power. RIS, which is constituted of a number of cost-effective passive reflectors, can intelligently adjust the induced signals by a controller and thus reconfigure the wireless propagation environment. Hence, RIS can improve communication performance by passive beamforming. Numerical studies have discussed the benefits of RIS-aided wireless communications. In [6], the authors proposed an RIS-assisted single-input single-output (SISO) communication system, whose ergodic capacity and outage probability are boosted by increasing the number of reflecting elements. In [7], the authors proposed an RIS-aided non-orthogonal multiple access (NOMA) communication system, whose performance gains can be improved by choosing the optimal reflection coefficients of the RIS.

In the studies of the UAV relaying communication system, the UAV trajectory optimization is extremely vital to maximize the system throughput. In [5], Zeng *et al.* proposed a mobile UAV relaying system and maximized the system throughput by jointly optimizing power allocation and UAV trajectory. With the RIS on the ground, integrated UAV and RIS wireless communication has been a promising research topic. A UAV-ground communication system was proposed in [8]–[10], where an RIS is adopted to enhance the communication peformance. Accordingly, the system throughput was maximized by jointly optimizing UAV trajectory and RIS passive beamforming.

The previous studies usually consider a static RIS on the ground to reflect the UAV signal, which cannot save the transmit power of the UAV. As for the RIS mounted on the UAV (RIS-UAV) to decrease the power consumption of the UAV, there are only a few studies at present such as [11]–[13]. In [11], the authors used RIS-UAV to achieve wider-view signal reflection. In [12], the authors adopted RIS-UAV to mitigate the jamming attacks and enhance the legitimate transmissions. But [11] and [12] both assumed that the RIS-UAV was in a fixed position and then found an optimal position for the RIS-UAV via deployment optimization. In [13], the authors proposed an RIS-UAV relaying model to improve cooperative communication performance. However, [13] assumed that the horizontal position of the RIS-UAV was fixed and maximized the communication performance via optimizing UAV's height.

In this paper, RIS-UAV serves as a mobile relay to conduct the classic three-node cooperative communication model, and the RIS-UAV trajectory is optimized to improve cooperative communication performance. The contributions of the paper are listed as follows.

- An RIS-UAV enabled cooperative communication system

Manuscript received xx, xxxx; revised August xx, xxxx. This work was supported in part by the Natural Science Foundations of Liaoning Province under Grant 2019-ZD-0014 and Grant 2020-HYLH-13, in part by the Fundamental Research Funds for the Central Universities under Grant DUT21JC20, and in part by the National Research Foundation of Singapore under its Strategic Capability Research Centres Funding Initiative. Any opinions, findings and conclusions or recommendations expressed in this material are those of the authors and do not reflect the views of National Research Foundation of Singapore. (*Correspondence author: Feng Li*)

X. Liu and Y. F. Yu are with the School of Information and Communication Engineering, Dalian University of Technology, Dalian 116024, China (e-mail: liuxinstar1984@dlut.edu.cn; yyf99s@163.com).

F. Li is with the School of Information and Electronic Engineering, Zhejiang Gongshang University, Hangzhou, 310018, China. He is also with the School of Computer Science and Engineering, Nanyang Technological University, 639798, Singapore (e-mail: fengli2002@yeah.net).

T. S. Durrani is with the Department of Electronic and Electrical Engineering, University of Strathclyde, Glasgow G1 1XQ, U.K. (e-mail: t.durrani@strath.ac.uk).

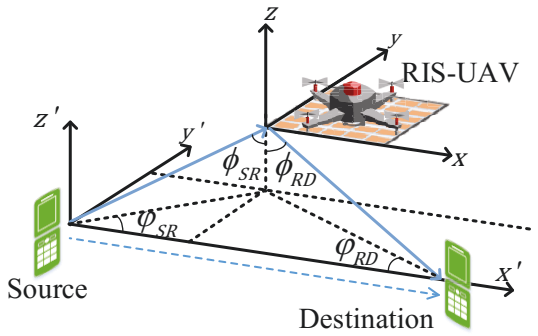

Fig. 1: RIS-UAV enabled cooperative communication model.

is presented, where the RIS is mounted on the UAV to passively reflect the source signal to the destination as a relay with less power consumption. A source-to-destination throughput maximization problem is formulated to jointly optimize source power allocation, UAV trajectory and RIS passive beamforming.

- The formulated non-convex optimization problem is first divided into three subproblems: passive beamforming optimization, UAV trajectory optimization and power allocation optimization. For the given source power and UAV trajectory, we derive a closed-form expression for the optimal RIS phase shift. For the given source power and RIS phase shift, we optimize the UAV trajectory via the first-order Taylor expansion of the objective function. For the given RIS phase shift and UAV trajectory, we use the standard convex optimization method to optimize the source power allocation. Finally, we propose an alternating iterative optimization algorithm of the three subproblems to obtain the suboptimal solutions.

II. System Model

Fig. 1 shows a three-node cooperative communication model constituting of Source, Destination and RIS-UAV mobile relay. The RIS-UAV can passively reflect the source signal to the destination with less power consumption. The horizontal coordinates of Source and Destination are denoted by $\boldsymbol{W}_s = \{x_s, y_s\}^T$ and $\boldsymbol{W}_d = \{x_d, y_d\}^T$, respectively. For simplicity, the RIS-UAV flies in the horizontal plane with a specific height H_0 within a finite flying time T. And T is discretized into N time slots, and thus $T = N\delta$ where δ denotes the slot width. The horizontal coordinate of the RIS-UAV in slot n is defined as $\boldsymbol{l}[n] = \{x_r[n], y_r[n]\}^{\mathrm{T}}, n \in \boldsymbol{\mathcal{N}} = \{1, 2, \ldots, N\}$. To approximate the real trajectory, $\boldsymbol{l}[n]$ should satisfy

$$\|\boldsymbol{l}[n+1] - \boldsymbol{l}[n]\|^2 \leq D^2, n = 1, 2, \ldots, N-1, \tag{1a}$$

$$\|\boldsymbol{l}[1] - \boldsymbol{l}_0\|^2 \leq D^2, \tag{1b}$$

$$\|\boldsymbol{l}_F - \boldsymbol{l}[N]\|^2 \leq D^2, \tag{1c}$$

where $\boldsymbol{l}_0$ and $\boldsymbol{l}_F$ represent the initial and final coordinates of the RIS-UAV, respectively, $D = v_{max}\delta$ is the maximum flying distance within one time slot, and v_{max} is the maximum UAV speed.

The power allocation of the Source for each time slot plays an important role in the cooperative communication performance and should be optimally solved. Let vector $\boldsymbol{p} \triangleq \{p[n], n \in \boldsymbol{\mathcal{N}}\}$ denote transmit power in each time slot, which should satisfy

$$\frac{1}{N}\sum_{n\in\boldsymbol{\mathcal{N}}} p[n] \leq P_{avg} \tag{2}$$

$$p[n] \geq 0, n \in \boldsymbol{\mathcal{N}}, \tag{3}$$

where P_{avg} is the average transmit power per time slot.

The RIS has a uniform planar array (UPA) and consists of $M = m \times m$ passive reflecting elements, whose phase shift in each time slot will affect the system throughput and is denoted by a diagonal phase-shift matrix $\boldsymbol{\Theta}[n] = \mathrm{diag}\{e^{j\theta_{(0,0)}[n]}, \ldots, e^{j\theta_{(p,q)}[n]}, \ldots, e^{j\theta_{(m-1,m-1)}[n]}\}, n \in \boldsymbol{\mathcal{N}}$. $\theta_{(p,q)}[n] \in [0, 2\pi)$ for $0 \leqslant p, q \leqslant m-1$ represents the phase shift of the (p,q)th RIS element in the nth slot, where (p,q) denotes the position of the passive element in the array and is set in a continuous manner between 0 and 2π by the RIS controller.

Since the flying altitude of the RIS-UAV is high enough, both the link between Source and RIS-UAV (S-R link) and the link between RIS-UAV and Destination (R-D link) are considered to be LoS. Hence, the S-R link gain in the nth slot, $\boldsymbol{h}_{SR}[n]$, can be given by

$$\boldsymbol{h}_{SR}[n] = \sqrt{\rho d_{SR}^{-\tau}[n]}\{1, \ldots, e^{-j\frac{2\pi}{\lambda}\chi\alpha_{SR}^{(p,q)}[n]}, \ldots, e^{-j\frac{2\pi}{\lambda}\chi\alpha_{SR}^{(m-1,m-1)}[n]}\}^{\mathrm{T}}, \tag{4}$$

where ρ represents the path loss at the unit distance $D_0 =$ 1m, τ denotes the path loss exponent of the S-R link, $d_{SR}[n] = \sqrt{H_0^2 + \|\boldsymbol{l}[n] - \boldsymbol{W}_s\|^2}$, χ and λ represent the antenna separation and carrier wavelength, respectively; $\alpha_{SR}^{(p,q)}[n] = p\sin\phi_{SR}[n]\sin\varphi_{SR}[n] + q\cos\phi_{SR}[n]\sin\varphi_{SR}[n]$, for $0 \leqslant p, q \leqslant m-1$ [14], where $\phi_{SR}[n]$ and $\varphi_{SR}[n]$ represent the azimuth and elevation angle of arrival (AOA) from the Source to the RIS-UAV in the time slot n, respectively.

The R-D link gain in the nth slot, $\boldsymbol{h}_{RD}[n]$, can likewise be given by

$$\boldsymbol{h}_{RD}[n] = \sqrt{\rho d_{RD}^{-\kappa}[n]}\{1, \ldots, e^{-j\frac{2\pi}{\lambda}\chi\alpha_{RD}^{(p,q)}[n]}, \ldots, e^{-j\frac{2\pi}{\lambda}\chi\alpha_{RD}^{(m-1,m-1)}[n]}\}^{\mathrm{T}}, \tag{5}$$

where κ denotes the path loss exponent of the R-D link, $d_{RD}[n] = \sqrt{H_0^2 + \|\boldsymbol{l}[n] - \boldsymbol{W}_d\|^2}$; $\alpha_{RD}^{(p,q)}[n] = p\sin\phi_{RD}[n]\sin\varphi_{RD}[n] + q\cos\phi_{RD}[n]\sin\varphi_{RD}[n]$, where $\phi_{RD}[n]$ and $\varphi_{RD}[n]$ represent the azimuth and elevation angle of departure (AOD) from the RIS-UAV to the Destination in the time slot n, respectively.

Though the link between the Source and the Destination (S-D link) may be blocked, there still exists scattered signals, and thus the channel can be modeled as Rayleigh fading. The channel gain, $\boldsymbol{h}_{SD}$, can be expressed as

$$h_{SD} = \sqrt{\rho d_{SD}^{-\alpha}}\tilde{h}, \tag{6}$$

where α denotes the path loss exponent of the S-D link, $d_{SD} =$

$\sqrt{\|\boldsymbol{W}_d - \boldsymbol{W}_s\|^2}$, and $\tilde{h}$ is the random scattering component modeled by a circularly symmetric complex Gaussian (CSCG) distribution with zero mean and unit variance.

With $(4)-(6)$, the signal-to-noise ratio (SNR) in each slot can be expressed by

$$\gamma_{SD}[n] = \frac{p[n]|h_{SD} + \boldsymbol{h}_{RD}[n]^{\boldsymbol{H}}\boldsymbol{\Theta}[n]\boldsymbol{h}_{SR}[n]|^2}{\sigma^2} \tag{7}$$

where σ^2 denotes the noise power. We can get the achievable throughput in bits/second/Hertz as follows

$$R_{SD}[n] = \log_2(1+\gamma_{SD}[n]) \tag{8}$$

Then the total throughput for N slots can be given by

$$R = \sum_{n\in\boldsymbol{\mathcal{N}}} R_{SD}[n] \tag{9}$$

III. Problem Formulation

In this paper, we aim to maximize the throughput R by jointly optimizing the power allocation $\boldsymbol{p} \triangleq \{p[n], n \in \boldsymbol{\mathcal{N}}\}$, the passive beamforming $\boldsymbol{\Phi} \triangleq \{\boldsymbol{\Theta}[n], n \in \boldsymbol{\mathcal{N}}\}$ and the UAV trajectory $\boldsymbol{L} \triangleq \{\boldsymbol{l}[n], n \in \boldsymbol{\mathcal{N}}\}$. The optimization problem is given by

$$\begin{aligned}
(\text{P1}): \max_{(\boldsymbol{p},\boldsymbol{\Phi},\boldsymbol{L})} \; & R \\
s.t. \; & 0 \le \theta_{(p,q)}[n] < 2\pi, \forall p,q,n, \qquad (10)\\
& \|\boldsymbol{l}[n+1] - \boldsymbol{l}[n]\|^2 \le D^2, n = 1,2,\ldots,N-1, \\
& \|\boldsymbol{l}[1] - \boldsymbol{l}_0\|^2 \le D^2, \\
& \|\boldsymbol{l}_F - \boldsymbol{l}[N]\|^2 \le D^2, \\
& \frac{1}{N}\sum_{n\in\boldsymbol{\mathcal{N}}} p[n] \le P_{avg}, \\
& p[n] \ge 0, n \in \boldsymbol{\mathcal{N}}
\end{aligned}$$

However, the objective function of (P1) is non-convex with regard to $\boldsymbol{p}, \boldsymbol{\Phi}, \boldsymbol{L}$, which cannot be solved by the standard convex optimization. In the following section, we separate (P1) into three subproblems and use the alternating iterative optimization to obtain the suboptimal solutions.

IV. Solution Algorithm

In this section, we divide the formulated optimization problem into three subproblems: power allocation optimization with fixed trajectory and reflection coefficient, reflection coefficient optimization with given power allocation and trajectory, and trajectory optimization with fixed power allocation and reflection coefficient. Furthermore, an alternating iterative optimization algorithm of the three subproblems is proposed to get the suboptimal solutions for (P1).

A. Power Allocation Optimization

With the given UAV trajectory and RIS reflection coefficients, the problem (P1) can be rewritten by

$$\begin{aligned}
(\text{P2}): \max_{\boldsymbol{p}} \; & \sum_{n\in\boldsymbol{\mathcal{N}}} \log_2(1+p[n]\gamma_0[n]) \\
s.t. \; & \frac{1}{N}\sum_{n\in\boldsymbol{\mathcal{N}}} p[n] \le P_{avg}, \\
& p[n] \ge 0, n \in \boldsymbol{\mathcal{N}}
\end{aligned}$$

where $\gamma_0[n] \triangleq \frac{|h_{SD}+\boldsymbol{h}_{RD}[n]^{\boldsymbol{H}}\boldsymbol{\Theta}[n]\boldsymbol{h}_{SR}[n]|^2}{\sigma^2}$ is a constant with the fixed trajectory and reflection coefficients. (P2) is a convex optimization problem and can be solved efficiently by standard convex optimization solvers such as CVX [15].

B. Passive Beamforming

When the trajectory and the power allocation are given, the channel gain $h_{SD} + \boldsymbol{h}_{RD}[n]^{\boldsymbol{H}}\boldsymbol{\Theta}[n]\boldsymbol{h}_{SR}[n]$ plays a leading role in the optimization. The maximum channel gain can be achieved when h_{SD} and $\boldsymbol{h}_{RD}[n]^{\boldsymbol{H}}\boldsymbol{\Theta}[n]\boldsymbol{h}_{SR}[n]|^2$ have the same phase.

Let $G[n]$ denote $h_{SD} + \boldsymbol{h}_{RD}[n]^{\boldsymbol{H}}\boldsymbol{\Theta}[n]\boldsymbol{h}_{SR}[n]$, which is further rewritten as follows

$$G[n] = \frac{\sqrt{\rho}}{d_{SD}^{\frac{\alpha}{2}}}\tilde{h} + \frac{\rho\sum_{p=0}^{m-1}\sum_{q=0}^{m-1} e^{j(\theta_{(p,q)}[n] - \frac{2\pi}{\lambda}\chi(\alpha_{SR}^{(p,q)}[n] - \alpha_{RD}^{(p,q)}[n]))}}{d_{SR}^{\frac{\tau}{2}}[n]d_{RD}^{\frac{\kappa}{2}}[n]} \tag{11}$$

Thus, we can get the optimal reflection coefficients with the given trajectory as follows

$$\theta_{(p,q)}[n] = \theta_{\tilde{h}} + \frac{2\pi}{\lambda}\chi(\alpha_{SR}^{(p,q)}[n] - \alpha_{RD}^{(p,q)}[n]), \forall p,q,n, \tag{12}$$

where $\theta_{\tilde{h}} = \arg(\tilde{h})$.

C. Trajectory Optimization

After optimizing the reflection coefficients, the channel gain can be expressed as follows

$$|G[n]| = \frac{\sqrt{\rho}}{d_{SD}^{\frac{\alpha}{2}}}|\tilde{h}| + \frac{M\rho}{d_{SR}^{\frac{\tau}{2}}[n]d_{RD}^{\frac{\kappa}{2}}[n]} \tag{13}$$

Then, (P1) can be reformulated by

$$\begin{aligned}
(\text{P3}): \max_{\boldsymbol{L}} \; & \sum_{n\in\boldsymbol{\mathcal{N}}} \log_2\left(1+\gamma[n]\left(\frac{\sqrt{\rho}}{d_{SD}^{\frac{\alpha}{2}}}|\tilde{h}| + \frac{M\rho}{d_{SR}^{\frac{\tau}{2}}[n]d_{RD}^{\frac{\kappa}{2}}[n]}\right)^2\right) \\
s.t. \; & \|\boldsymbol{l}[n+1] - \boldsymbol{l}[n]\|^2 \le D^2, n = 1,2,\ldots,N-1, \\
& \|\boldsymbol{l}[1] - \boldsymbol{l}_0\|^2 \le D^2, \\
& \|\boldsymbol{l}_F - \boldsymbol{l}[N]\|^2 \le D^2,
\end{aligned}$$

where $\gamma[n] \triangleq \frac{p[n]}{\sigma^2}$ denotes the SNR in the transmitter. However, the problem (P3) is still non-convex with respect to $\boldsymbol{L}$. To solve (P3), the slack variables $\boldsymbol{u} \triangleq \{u[n]\}, n \in \boldsymbol{\mathcal{N}}$ and $\boldsymbol{v} \triangleq \{v[n]\}, n \in \boldsymbol{\mathcal{N}}$ are introduced to relax $d_{SR}[n]$ and $d_{RD}[n]$, respectively. Then (P3) can be reformulated as follows

$$\begin{aligned}
(\text{P4}): \max_{\boldsymbol{L},\boldsymbol{u},\boldsymbol{v}} \; & \sum_{n\in\boldsymbol{\mathcal{N}}} \log_2\left(1+\gamma[n]\left(\frac{\sqrt{\rho}}{d_{SD}^{\frac{\alpha}{2}}}|\tilde{h}| + \frac{M\rho}{u^{\frac{\tau}{2}}[n]v^{\frac{\kappa}{2}}[n]}\right)^2\right) \\
s.t. \; & u[n] \ge d_{SR}[n], \forall n, \qquad (14)\\
& v[n] \ge d_{RD}[n], \forall n, \qquad (15)\\
& \|\boldsymbol{l}[n+1] - \boldsymbol{l}[n]\|^2 \le D^2, n = 1,2,\ldots,N-1, \\
& \|\boldsymbol{l}[1] - \boldsymbol{l}_0\|^2 \le D^2, \\
& \|\boldsymbol{l}_F - \boldsymbol{l}[N]\|^2 \le D^2,
\end{aligned}$$

To achieve the maximum value of (P4), the two constraints (14) and (15) must hold the equality. Otherwise, the increase of $\boldsymbol{u}$ and $\boldsymbol{v}$ will decrease the objective value. Thus, (P3) and (P4) have the same optimal solutions. Then we give the Lemma 1 to solve (P4).

Lemma 1: With given $Q_1 > 0$, $Q_2 > 0$, $Q_3 > 0$, $\tau > 0$, and $\kappa > 0$, the function $f(x, y) = \log_2(Q_1 + \frac{Q_2}{x^{\frac{\tau}{2}} y^{\frac{\kappa}{2}}} + \frac{Q_3}{x^{\tau} y^{\kappa}})$ is convex with respect to $x > 0$ and $y > 0$.

Proof: See Appendix A. ∎

Then, the slack convex objective function of (P4) is given by

$$R_{slack}[n] = \log_2\left(Q_1[n] + \frac{Q_2[n]}{u^{\frac{\tau}{2}}[n] v^{\frac{\kappa}{2}}[n]} + \frac{Q_3[n]}{u^{\tau}[n] v^{\kappa}[n]}\right) \quad (16)$$

where $Q_1[n] = 1 + \frac{\gamma[n]\rho|\tilde{h}|}{d_{SD}^{\alpha}}$, $Q_2[n] = \frac{2M\gamma[n]\rho^{\frac{3}{2}}|\tilde{h}|}{d_{SD}^{\alpha/2}}$ and $Q_3[n] = \gamma[n]M^2\rho^2$. By applying the first-order Taylor expansion to the objective function, it will become a linear function that can be solved by the CVX. The first-order Taylor expansion of $\boldsymbol{u}$, $\boldsymbol{v}$ and R_{slack} at the fixed point $\boldsymbol{u}_0 = \{u_0[n]\}_{n=1}^N$ and $\boldsymbol{v}_0 = \{v_0[n]\}_{n=1}^N$ are given as follows

$$-u^2[n] \le u_0^2[n] - 2u[n]u_0[n] \quad (17)$$

$$-v^2[n] \le v_0^2[n] - 2v[n]v_0[n] \quad (18)$$

$$R_{slack}[n] \ge A_0[n] + B_0[n](u[n] - u_0[n]) + C_0[n](v[n] - v_0[n]) \quad (19)$$

where

$$A_0[n] = \log_2(Q_1[n] + \frac{Q_2[n]}{u_0^{\frac{\tau}{2}}[n] v_0^{\frac{\kappa}{2}}[n]} + \frac{Q_3[n]}{u_0^{\tau}[n] v_0^{\kappa}[n]}) \quad (20)$$

$$B_0[n] = \frac{-\frac{\tau}{2}Q_2[n]u_0^{\frac{\tau}{2}-1}[n]v_0^{\frac{\kappa}{2}}[n] - \tau Q_3[n]u_0^{-1}[n]}{\ln 2(Q_1[n]u_0^{\tau}[n]v_0^{\kappa}[n] + Q_2[n]u_0^{\frac{\tau}{2}}[n]v_0^{\frac{\kappa}{2}}[n] + Q_3[n])} \quad (21)$$

$$C_0[n] = \frac{-\frac{\kappa}{2}Q_2[n]u_0^{\frac{\tau}{2}}[n]v_0^{\frac{\kappa}{2}-1}[n] - \kappa Q_3[n]v_0^{-1}[n]}{\ln 2(Q_1[n]u_0^{\tau}[n]v_0^{\kappa}[n] + Q_2[n]u_0^{\frac{\tau}{2}}[n]v_0^{\frac{\kappa}{2}}[n] + Q_3[n])} \quad (22)$$

According to (17), (18) and (19), (P4) can be rewritten by

$$\begin{aligned}
(\text{P5}): \max_{\boldsymbol{L},\boldsymbol{u},\boldsymbol{v}} & \sum_{n\in\boldsymbol{\mathcal{N}}} B_0[n]u[n] + C_0[n]v[n] \\
s.t.\ & d_{SR}^2[n] + u_0^2[n] - 2u[n]u_0[n] \le 0, \forall n, \quad (23) \\
& d_{RD}^2[n] + v_0^2[n] - 2v[n]v_0[n] \le 0, \forall n, \quad (24) \\
& \|\boldsymbol{l}[n+1] - \boldsymbol{l}[n]\|^2 \le D^2, n = 1, 2, \ldots, N-1, \\
& \|\boldsymbol{l}[1] - \boldsymbol{l}_0\|^2 \le D^2, \\
& \|\boldsymbol{l}_F - \boldsymbol{l}[N]\|^2 \le D^2,
\end{aligned}$$

which is convex and can be solved by the CVX [15]. By alternatingly optimizing the above three subproblems, the trajectory, power allocation and passive beamforming are jointly optimized in the Algorithm 1.

Lemma 2: Algorithm 1 is guaranteed to be convergent after enough iterations.

Proof: See Appendix B. ∎

V. Numerical Results

The simulation parameters are set as follows. The Cartesian coordinates of the Source and the Destination are (0, 0, 0) and (1000, 0, 0), respectively. The initial and final location coordinates of the RIS-UAV are (200, 50, 70) and (800, 50, 70), respectively. The maximum velocity of the UAV is 30m/s. The path loss at $D_0 = 1$m is -20dB. And the rest of the parameters are δ = 1s, σ^2 = -90dBm, $\chi = \frac{\lambda}{2}$, $\alpha = 2.5$, $\tau = 2$, $N = 200$, $M = 100$ and $P_{avg} = 20$mW. Commonly, the size of one RIS element is $8mm \times 8mm$ [16]. Therefore, an RIS plane with $M = 100$ elements has the size of $8cm \times 8cm$ and can be mounted on a UAV.

Algorithm 1 Alternating iterative optimization algorithm for solving (P1).

Initialize: the iteration number $m = 0$, $\{\boldsymbol{L}^{[m]}, \boldsymbol{\Phi}^{[m]}, \boldsymbol{p}^{[m]}, \boldsymbol{u}^{[m]}, \boldsymbol{v}^{[m]}\}$ with any positive values, the average throughput $R^{[m]}$ with the given $\{\boldsymbol{L}^{[m]}, \boldsymbol{\Phi}^{[m]}, \boldsymbol{p}^{[m]}, \boldsymbol{u}^{[m]}, \boldsymbol{v}^{[m]}\}$;

1: **while** R is not convergent **do**
2: update $\boldsymbol{L}^{[m+1]}, \boldsymbol{u}^{[m+1]}, \boldsymbol{v}^{[m+1]}$ by solving problem (P5);
3: update $\boldsymbol{p}^{[m+1]}$ by solving problem (P2);
4: update $\boldsymbol{\Phi}^{[m+1]}$ by (13);
5: calculate $R^{[m+1]}$ according to (7) and (8);
6: set $m = m + 1$;
7: **end while**

Output: the optimal solutions $\boldsymbol{L}^{[m]}, \boldsymbol{\Phi}^{[m]}, \boldsymbol{p}^{[m]}$.

Fig. 2 illustrates the optimal UAV trajectory with respect to different path loss exponents of the R-D link. If the path loss exponent of the R-D link, κ, is less than that of the S-R link, τ, the optimal hovering position is over the Source. If $\kappa > \tau$ (Fig. 2 (a): $\kappa = 2.5, \tau = 2$), the optimal hovering position is over the Destination. If $\kappa = \tau$ (Fig. 2 (b)), the RIS-UAV will travel from the Source to the Destination and hover over both the two positions. That is because the optimal UAV trajectory prefers the low-loss path to achieve higher system throughput. In addition, when $\kappa < \tau$ (Fig. 2(a): $\kappa = 1.2, \tau = 2$), to guarantee better relaying performance, the RIS-UAV will try to approach the destination when departing from the Source to the final position.

Fig. 3 illustrates the optimal power allocation for the Source in each time slot when $\kappa = \tau$. The RIS-UAV hovers over both the Source and the Destination. It is seen that when the power is mainly distributed for the hovering time (7th-83rd slots over the Source and 117th-194th slots over the Destination), the RIS-UAV can achieve better communication performance.

Fig. 4 illustrates the achievable throughput when $\kappa = \tau$ with respect to different time slots versus some UAV relay models with $P_{avg} = 20$mW: the proposed mobile RIS-UAV relay model with trajectory optimization, the mobile RIS-UAV model without trajectory optimization (UAV directly flies to the final position), and the static RIS-UAV relay model [13] hovering at the fixed position (500,0,70) in the middle of the Source and Destination. We can see that the throughput for the mobile RIS-UAV relay with trajectory optimization improves with the time and is always larger than that of the other two models. Because the UAV trajectory of the proposed model tends to be the optimal trajectory for maximizing the throughput with the increase of the time slots.

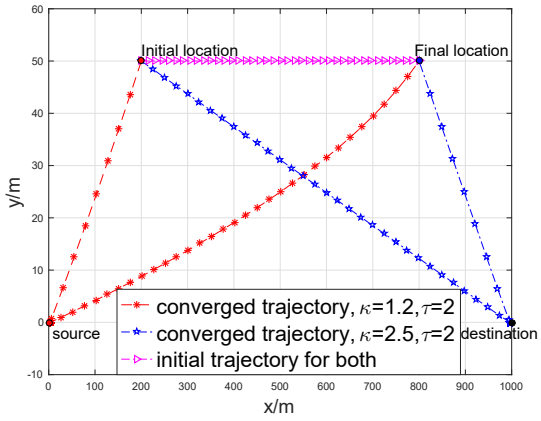

(a)

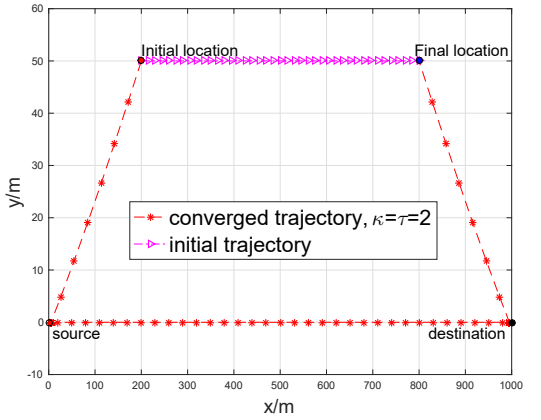

(b)

Fig. 2: UAV trajectory with respect to different path loss exponents for R-D link: (a) $\kappa \neq \tau$; (b) $\kappa = \tau$.

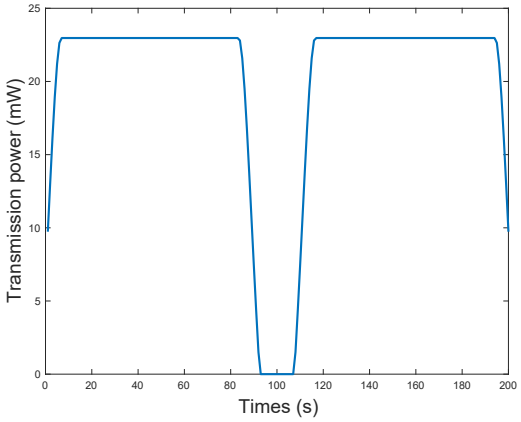

Fig. 3: Optimal power allocation for each time slot

VI. Conclusions

In this paper, an RIS-UAV relaying communication system is proposed to assist the ground communications, where the RIS-UAV serves as a passive and mobile relay to perform cooperative communications between the Source and the Destination. The system throughput is maximized by formulating a joint optimization problem of RIS passive beamforming, UAV trajectory and power allocation of the Source. The non-convex optimization problem is divided into three subproblems: passive beamforming optimization, UAV trajectory optimization and power allocation optimization. An alternating iterative optimization algorithm is proposed to achieve the suboptimal solutions by iteratively optimizing the three subproblems. The numerical results show that the RIS-UAV relaying communication with trajectory optimization can achieve better performance with enough RIS elements.

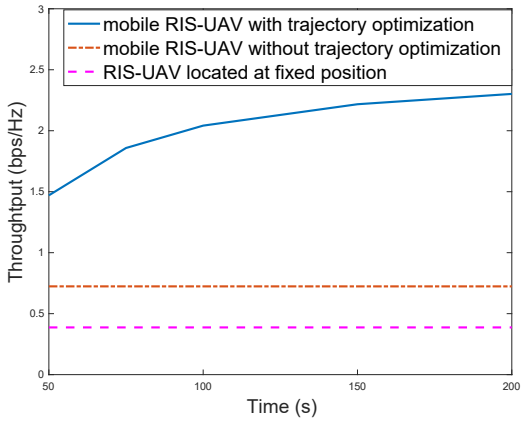

Fig. 4: Achievable throughput versus different UAV models.

Appendix A
Proof of Lemma 1

The first-order partial derivatives of $f(x, y)$ in x and y are respectively calculated as follows

$$\frac{\partial f}{\partial x} = \frac{-\frac{\tau}{2} Q_2 x^{\frac{\tau}{2}-1} y^{\frac{\kappa}{2}} - \tau Q_3 x^{-1}}{\ln 2 (Q_1 x^{\tau} y^{\kappa} + Q_2 x^{\frac{\tau}{2}} y^{\frac{\kappa}{2}} + Q_3)} \tag{25}$$

$$\frac{\partial f}{\partial y} = \frac{-\frac{\kappa}{2} Q_2 x^{\frac{\tau}{2}} y^{\frac{\kappa}{2}-1} - \kappa Q_3 y^{-1}}{\ln 2 (Q_1 x^{\tau} y^{\kappa} + Q_2 x^{\frac{\tau}{2}} y^{\frac{\kappa}{2}} + Q_3)} \tag{26}$$

And the second-order partial derivatives of $f(x, y)$ are calculated by (27)-(29) at the top of the next page. Accordingly, the Hessian matrix of $f(x, y)$ is given by

$$\bigtriangledown^2 f = \begin{bmatrix} \frac{\partial^2 f}{\partial x^2} & \frac{\partial^2 f}{\partial x \partial y} \\ \frac{\partial^2 f}{\partial y \partial x} & \frac{\partial^2 f}{\partial y^2} \end{bmatrix} \tag{30}$$

we can see $\frac{\partial^2 f}{\partial x^2} > 0$ and $\frac{\partial^2 f}{\partial x^2} \frac{\partial^2 f}{\partial y^2} - \frac{\partial^2 f}{\partial x \partial y} \frac{\partial^2 f}{\partial y \partial x} > 0$. Hence, $\bigtriangledown^2 f$ is positive definite, which indicates that $f(x, y)$ is a convex function.

Appendix B
Proof of Lemma 2

Let $\eta(\boldsymbol{p}^{(m)}, \boldsymbol{\Phi}^{(m)}, \boldsymbol{L}^{(m)})$ be the objective value of problem (P1) in the mth iteration for $m \geqslant 1$. Likewise, $\xi(\boldsymbol{p}^{(m)}, \boldsymbol{\Phi}^{(m)}, \boldsymbol{L}^{(m)}, \boldsymbol{u}^{(m)}, \boldsymbol{v}^{(m)})$ and $\xi_{lb}(\boldsymbol{p}^{(m)}, \boldsymbol{\Phi}^{(m)}, \boldsymbol{L}^{(m)}, \boldsymbol{u}^{(m)}, \boldsymbol{v}^{(m)})$ denote the objective

$$\frac{\partial^2 f}{\partial x^2} = \frac{(\frac{\tau^2}{4}+\frac{\tau}{2})Q_1Q_2x^{\frac{3}{2}\tau-2}y^{\frac{3}{2}\kappa}+(\frac{\tau}{2}Q_2^2+(\tau^2+\tau)Q_1Q_3)x^{\tau-2}y^{\kappa}+(\frac{\tau^2}{4}+\frac{3\tau}{2})Q_2Q_3x^{\frac{\tau}{2}-2}y^{\frac{\kappa}{2}}+\tau Q_3^2x^{-2}}{\ln 2(Q_1x^{\tau}y^{\kappa}+Q_2x^{\frac{\tau}{2}}y^{\frac{\kappa}{2}}+Q_3)^2} \tag{27}$$

$$\frac{\partial^2 f}{\partial y^2} = \frac{(\frac{\kappa^2}{4}+\frac{\kappa}{2})Q_1Q_2x^{\frac{3}{2}\tau}y^{\frac{3}{2}\kappa-2}+(\frac{\kappa}{2}Q_2^2+(\kappa^2+\kappa)Q_1Q_3)x^{\tau}y^{\kappa-2}+(\frac{\kappa^2}{4}+\frac{3\kappa}{2})Q_2Q_3x^{\frac{\tau}{2}}y^{\frac{\kappa}{2}-2}+\kappa Q_3^2y^{-2}}{\ln 2(Q_1x^{\tau}y^{\kappa}+Q_2x^{\frac{\tau}{2}}y^{\frac{\kappa}{2}}+Q_3)^2} \tag{28}$$

$$\frac{\partial^2 f}{\partial x\partial y} = \frac{\partial^2 f}{\partial y\partial x} = \frac{\frac{\tau\kappa}{4}Q_1Q_2x^{\frac{3\tau}{2}-1}y^{\frac{3\kappa}{2}-1}+\tau\kappa Q_1Q_3x^{\tau-1}y^{\kappa-1}+\frac{\tau\kappa}{4}Q_2Q_3x^{\frac{\tau}{2}-1}y^{\frac{\kappa}{2}-1}}{\ln 2(Q_1x^{\tau}y^{\kappa}+Q_2x^{\frac{\tau}{2}}y^{\frac{\kappa}{2}}+Q_3)^2} \tag{29}$$

values of problems (P4) and (P5), respectively. In the step 2 of the Algorithm 1, we can get the inequality as

$$\begin{aligned}
&\eta(\boldsymbol{p}^{(m-1)}, \boldsymbol{\Phi}^{(m-1)}, \boldsymbol{L}^{(m-1)}) \\
&= \xi(\boldsymbol{p}^{(m-1)}, \boldsymbol{\Phi}^{(m-1)}, \boldsymbol{L}^{(m-1)}, \boldsymbol{u}^{(m-1)}, \boldsymbol{v}^{(m-1)}) && \text{(31a)} \\
&= \xi_{lb}(\boldsymbol{p}^{(m-1)}, \boldsymbol{\Phi}^{(m-1)}, \boldsymbol{L}^{(m-1)}, \boldsymbol{u}^{(m-1)}, \boldsymbol{v}^{(m-1)}) && \text{(31b)} \\
&\leqslant \xi_{lb}(\boldsymbol{p}^{(m-1)}, \boldsymbol{\Phi}^{(m-1)}, \boldsymbol{L}^{(m)}, \boldsymbol{u}^{(m)}, \boldsymbol{v}^{(m)}) && \text{(31c)} \\
&\leqslant \xi(\boldsymbol{p}^{(m-1)}, \boldsymbol{\Phi}^{(m-1)}, \boldsymbol{L}^{(m)}, \boldsymbol{u}^{(m)}, \boldsymbol{v}^{(m)}) && \text{(31d)} \\
&= \eta(\boldsymbol{p}^{(m-1)}, \boldsymbol{\Phi}^{(m-1)}, \boldsymbol{L}^{(m)}) && \text{(31e)}
\end{aligned}$$

where (31a) and (31e) hold because problems (P3) and (P4) have the same optimal solution of $\boldsymbol{L}$; (31b) holds because the first-order Taylor expansions of (17), (18) and (19) are tight at the feasible point $(\boldsymbol{L}_{fea}, \boldsymbol{u}_{fea}, \boldsymbol{v}_{fea}) = (\boldsymbol{L}^{(m-1)}, \boldsymbol{u}^{(m-1)}, \boldsymbol{v}^{(m-1)})$; (31c) holds because $(\boldsymbol{L}^{(m)}, \boldsymbol{u}^{(m)}, \boldsymbol{v}^{(m)})$ is the optimal solution to problem (P5); (31d) holds because the objective value of problem (P5) is a lower bound of that of problem (P4). Since we can get the optimal solution of power allocation after solving problem (P2), in the step 3 of the Algorithm 1, we can get the inequality as

$$\eta(\boldsymbol{p}^{(m-1)}, \boldsymbol{\Phi}^{(m-1)}, \boldsymbol{L}^{(m)}) \leqslant \eta(\boldsymbol{p}^{(m)}, \boldsymbol{\Phi}^{(m-1)}, \boldsymbol{L}^{(m)}) \tag{32}$$

Likewise, since we can get the optimal phase shifts of the RIS, in the step 4 of the Algorithm 1, we can get the inequality as

$$\eta(\boldsymbol{p}^{(m)}, \boldsymbol{\Phi}^{(m-1)}, \boldsymbol{L}^{(m)}) \leqslant \eta(\boldsymbol{p}^{(m)}, \boldsymbol{\Phi}^{(m)}, \boldsymbol{L}^{(m)}) \tag{33}$$

which means that the objective value of problem (P1) is non-decreasing over the iterations of the Algorithm 1. Since the optimal value of (P1) is upper-bounded by a finite value, the Algorithm 1 is guaranteed to converge.

REFERENCES

[1] B. Li, Z. Fei, Y. Zhang, and M. Guizani, "Secure UAV communication networks over 5G," *IEEE Wireless Communications*, vol. 26, no. 5, pp. 114–120, 2019.

[2] G. Gui, M. Liu, F. Tang, N. Kato, and F. Adachi, "6G: Opening new horizons for integration of comfort, security, and intelligence," *IEEE Wireless Communications*, vol. 27, no. 5, pp. 126–132, 2020.

[3] L. Gupta, R. Jain, and G. Vaszkun, "Survey of important issues in UAV communication networks," *IEEE Communications Surveys & Tutorials*, vol. 18, no. 2, pp. 1123–1152, 2016.

[4] Y. Xu, G. Gui, H. Gacanin, and F. Adachi, "A survey on resource allocation for 5G heterogeneous networks: Current research, future trends, and challenges," *IEEE Communications Surveys & Tutorials*, vol. 23, no. 2, pp. 668–695, 2021.

[5] Y. Zeng, R. Zhang, and T. J. Lim, "Throughput maximization for UAV-enabled mobile relaying systems," *IEEE Transactions on Communications*, vol. 64, no. 12, pp. 4983–4996, 2016.

[6] Q. Tao, J. Wang, and C. Zhong, "Performance analysis of intelligent reflecting surface aided communication systems," *IEEE Communications Letters*, vol. 24, no. 11, pp. 2464–2468, 2020.

[7] J. Zuo, Y. Liu, Z. Qin, and N. Al-Dhahir, "Resource allocation in intelligent reflecting surface assisted NOMA systems," *IEEE Transactions on Communications*, vol. 68, no. 11, pp. 7170–7183, 2020.

[8] S. Li, B. Duo, X. Yuan, Y. C. Liang, and M. Renzo, "Reconfigurable intelligent surface assisted UAV communication: Joint trajectory design and passive beamforming," *IEEE Wireless Communications Letters*, vol. 9, no. 5, pp. 716–720, 2020.

[9] H. Mei, K. Yang, J. Shen, and Q. Liu, "Joint trajectory-task-cache optimization with phase-shift design of RIS-assisted UAV for MEC," *IEEE Wireless Communications Letters*, vol. 10, no. 7, pp. 1586–1590, 2021.

[10] L. Ge, P. Dong, H. Zhang, J. B. Wang, and X. You, "Joint beamforming and trajectory optimization for intelligent reflecting surfaces-assisted UAV communications," *IEEE Access*, vol. 8, pp. 78 702–78 712, 2020.

[11] H. Lu, Y. Zeng, S. Jin, and R. Zhang, "Aerial intelligent reflecting surface: Joint placement and passive beamforming design with 3D beam flattening," *IEEE Transactions on Wireless Communications*, vol. 20, no. 7, pp. 4128–4143, 2021.

[12] X. Tang, D. Wang, R. Zhang, Z. Chu, and Z. Han, "Jamming mitigation via aerial reconfigurable intelligent surface: Passive beamforming and deployment optimization," *IEEE Transactions on Vehicular Technology*, vol. 70, no. 6, pp. 6232–6237, 2021.

[13] T. Shafique, H. Tabassum, and E. Hossain, "Optimization of wireless relaying with flexible UAV-borne reflecting surfaces," *IEEE Transactions on Communications*, vol. 69, no. 1, pp. 309–325, 2021.

[14] X. Guo, Y. Chen, and Y. Wang, "Learning-based robust and secure transmission for reconfigurable intelligent surface aided millimeter wave UAV communications," *IEEE Wireless Communications Letters*, vol. 10, no. 8, pp. 1795–1799, 2021.

[15] M. Grant and S. P. Boyd, "CVX: Matlab software for disciplined convex programming," *http://cvxr.com/cvx/*, 2020.

[16] J. Zhang, E. Bjrnson, M. Matthaiou, D. W. K. Ng, H. Yang, and D. J. Love, "Prospective multiple antenna technologies for beyond 5G," *IEEE Journal on Selected Areas in Communications*, vol. 38, no. 8, pp. 1637–1660, 2020.